

$J = 1/2$ Pseudospins and d - p Hybridization in the Kitaev Spin Liquid Candidates RuX_3 ($X = \text{Cl}, \text{Br}, \text{I}$)

H. Gretarsson,¹ H. Fujihara,² F. Sato,² H. Gotou,³ Y. Imai,² K. Ohgushi,² B. Keimer,⁴ and H. Suzuki^{5,6,*}

¹*Deutsches Elektronen-Synchrotron DESY, Notkestrasse 85, D-22607 Hamburg, Germany*

²*Department of Physics, Graduate School of Science, Tohoku University,*

6-3 Aramaki-Aoba, Aoba-ku, Sendai, Miyagi 980-8578, Japan

³*Institute for Solid State Physics (ISSP), University of Tokyo, Kashiwa, Chiba 277-8581, Japan*

⁴*Max-Planck-Institut für Festkörperforschung, Heisenbergstraße 1, D-70569 Stuttgart, Germany*

⁵*Frontier Research Institute for Interdisciplinary Sciences, Tohoku University, Sendai 980-8578, Japan*

⁶*Institute of Multidisciplinary Research for Advanced Materials (IMRAM), Tohoku University, Sendai 980-8577, Japan*

(Dated: March 1, 2024)

The recent synthesis of ruthenium trihalides RuX_3 ($X = \text{Cl}, \text{Br}, \text{I}$) has enlarged the set of material candidates for Kitaev spin liquid. The realization of Kitaev model necessitates the formation of $J = 1/2$ pseudospins in the octahedral crystal field. We use Ru L_3 -edge resonant inelastic x-ray scattering to investigate the evolution of multiplet structures in RuX_3 . We identified quasi-elastic magnetic correlations and spin-orbit transitions to the $J = 3/2$ states without discernible trigonal splitting, thereby validating the $J = 1/2$ description of magnetism in the RuX_3 family. Lineshape broadening in RuI_3 provides evidence for its bulk metallicity in the vicinity of a bandwidth-controlled metal-insulator transition. Our results highlight the pivotal role of halogen p orbitals in controlling the electronic properties of RuX_3 .

The exactly soluble Kitaev honeycomb model [1] embodies key concepts in modern condensed matter physics, such as quantum spin liquids, spin fractionalization, and emergent Majorana fermions. This model also holds promise as a basis for fault-tolerant quantum computation, which drives the search for its realization in physical platforms. The theoretical proposal of t_{2g}^5 spin-orbit Mott insulators as a solid-state platform of the Kitaev model [2] has spurred extensive research into magnetism in $4d/5d$ transition metal compounds [3–5]. The bond-dependent interaction in the Kitaev model can also emerge in the transition metal compounds with the high-spin d^7 electron configurations [6–8] and in the rare-earth magnets with an odd number of $4f$ electrons per site [9–11]. These theoretical proposals have expanded the list of candidate magnets whose syntheses have been already reported [8, 12]. The targeted synthesis effort requires experimental scrutiny to assess whether each candidate contains the essential ingredients of the Kitaev model.

Among the Kitaev spin liquid candidates, α - RuCl_3 (hereafter RuCl_3) has been a focus of extensive research since signatures of fractionalized excitations have been identified in Raman scattering [13], neutron scattering [14–17], and thermal transport experiments [18, 19]. However, the zigzag antiferromagnetic order at ~ 7 K [20] points to a certain deviation from the pure Kitaev model due to additional non-Kitaev interactions. In general, the nearest-neighbor interaction between the pseudospins on a z -bond, $\mathcal{H}_{ij}^{(z)}$, is expressed as [21, 22]

$$\begin{aligned} \mathcal{H}_{ij}^{(z)} = & K S_i^z S_j^z + J \mathbf{S}_i \cdot \mathbf{S}_j + \Gamma (S_i^x S_j^y + S_i^y S_j^x) \\ & + \Gamma' (S_i^x S_j^z + S_i^z S_j^x + S_i^y S_j^z + S_i^z S_j^y), \end{aligned} \quad (1)$$

where K is the bond-dependent Kitaev interaction, J is Heisenberg exchange, and Γ is the symmetric off-diagonal

exchange. The additional symmetric off-diagonal exchange Γ' becomes nonzero if the crystal field shows distortions from the cubic symmetry. For the $\gamma = x, y$ bonds, $\mathcal{H}_{ij}^{(\gamma)}$ follow from cyclic permutations of S_i^x, S_i^y, S_i^z . Recent resonant x-ray scattering studies [23, 24] have revealed the predominance of the ferromagnetic K term, while the subdominant J and Γ terms are necessary to describe the zigzag order [25]. Considering the proximity of RuCl_3 to the Kitaev model, the fine-tuning of the magnetic Hamiltonian of RuCl_3 provides a viable approach to the spin-liquid state.

As the Kitaev interaction stems from the electron hopping between the nearest-neighbor t_{2g} orbitals via the ligand p orbitals in the edge-shared octahedra [2], a natural strategy is to replace Cl with heavier halogen elements, such as Br and I. Indeed, the recent synthesis of the sibling compounds RuBr_3 [26–28] and RuI_3 [26, 29, 30], along with their solid solution $\text{Ru}(\text{Br}_{1-x}\text{I}_x)_3$ [31, 32], paves the way for the continuous tuning of the electronic properties. It is noteworthy that an insulator-to-metal transition occurs in $\text{Ru}(\text{Br}_{1-x}\text{I}_x)_3$ at the doping level of $x \sim 0.85$ [31, 32], placing RuI_3 in the metallic regime. Moreover, the introduction of polar structural asymmetry in the halogen site could stabilize an antiferromagnetic K term [33]. Despite the large tunability of magnetism in transition metal halides, the effect of the halogen substitution on the microscopic electronic properties remains to be resolved.

In this Letter, we report a systematic Ru L_3 -edge resonant inelastic x-ray scattering (RIXS) investigation of the multiplet structures in the ruthenium trihalides RuX_3 ($X = \text{Cl}, \text{Br}, \text{I}$). In all the RuX_3 systems, we observed pseudospin $J = 1/2$ quasi-elastic peaks and spin-orbit transitions to the $J = 3/2$ quartet without discernible trigonal

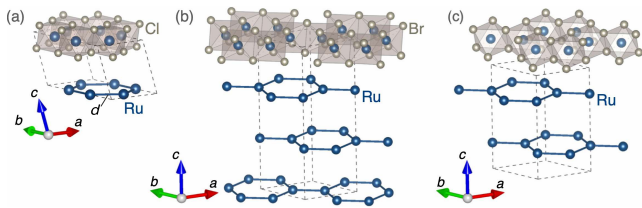


FIG. 1. Crystal structures of RuX_3 ($X = \text{Cl}, \text{Br}, \text{I}$). (a) AlCl_3 -type crystal structure (space group: $C2/m$) of $\alpha\text{-RuCl}_3$. (b) BiI_3 -type structure ($R\bar{3}$) of RuBr_3 . (c) Anti- Ti_3O -type structure ($P\bar{3}1c$) of RuI_3 . This figure is drawn using the VESTA software [34].

field splitting, validating the formation of the $J = 1/2$ pseudospins as the basis of the magnetism of RuX_3 . In the metallic RuI_3 , we identified lineshape broadening and the disappearance of the energy gap in the intersite charge continuum. This suggests that RuI_3 is located on the verge of a bandwidth-controlled metal-insulator transition. Multiplet analysis of the RIXS spectra reveals a systematic evolution of the crystal field parameters, due to the increase of the halogen p orbital contribution to the low-energy states as X goes from Cl to I. These results establish halogen substitution as an effective tuning knob for the bulk electronic properties of Kitaev magnets.

In addition to RuCl_3 single crystals, we employed RuBr_3 and RuI_3 polycrystals with honeycomb lattice structures grown by high-pressure synthesis [27, 29, 30]. We summarize in Fig. 1 the crystal structures of the RuX_3 employed in this work. While the space group of RuCl_3 at low temperature is still under debate [25, 35–37], there is a consensus that RuCl_3 at room temperature takes an AlCl_3 -type monoclinic crystal structure with a slightly distorted honeycomb lattice in the unit cell [$C2/m$, Fig. 1(a)]. The intralayer Ru-Ru bond lengths d are given by $d = 3.425 \text{ \AA}$ and 3.461 \AA . RuBr_3 has a BiI_3 -type structure below room temperature without structural transition [$R\bar{3}$, Fig. 1(b)] [27], where the three regular Ru honeycomb layers with $d = 3.639 \text{ \AA}$ in the unit cell form the ABCABC-type close-packed stacking sequence. For RuI_3 , different growth conditions yield two types of crystal structures [29, 30]. Our RuI_3 crystals have an anti- Ti_3O -type structure [$P\bar{3}1c$, Fig. 1(c)] [29], where the two regular honeycomb layers with $d = 3.913 \text{ \AA}$ form the ABAB-type stacking sequence. We will discuss how the increase of d affects the electronic properties below.

Figure 2(a) presents the scattering geometry of the RIXS experiment, which were conducted using the intermediate-energy RIXS (IRIXS) spectrometer at the Dynamics Beamline P01 of PETRA III, DESY [38]. We employed π -polarized x-ray photons with $h\nu = 2837$ and 2839 eV , close to the Ru L_3 absorption edge. Scattered photons were collected at a fixed scattering angle of 90° using a SiO_2 ($10\bar{2}$) diced spherical analyzer and a CCD

camera. The polarizations of the outgoing photons were not analyzed. The incident x-ray beam was focused to a beam spot of $20 \times 150 \mu\text{m}^2$ ($H \times V$). The exact position of zero energy loss and the energy resolution of $\Delta E \sim 80 \text{ meV}$ were determined by the center and the full width at half-maximum, respectively, of the nonresonant elastic signal from silver paint deposited next to the samples. For the measurement of the RuCl_3 single crystal, the sample angles were set to $\theta = 20^\circ$ and $\phi = 0^\circ$. For the RuBr_3 and RuI_3 polycrystals, the RIXS data reflect the geometrical average over the entire range of sample angles θ , ϕ , and the tilt angle χ (not drawn). All the measurements were performed at $T = 300 \text{ K}$, in the paramagnetic states of RuX_3 .

Figure 2(b) shows the Ru L_3 RIXS spectra of RuX_3 ($X = \text{Cl}, \text{Br}, \text{I}$) taken with incident photons with $h\nu = 2837 \text{ eV}$. The spectrum for RuCl_3 reproduces a previous result in Ref. [24]. At low energy, the spin-orbit transitions to the $J = 3/2$ states (circles) are identified in all the RuX_3 compounds. The peak energies for RuCl_3 and RuBr_3 are almost identical (0.25 eV), while it shifts to a higher energy of 0.3 eV in RuI_3 . The $J = 3/2$ peaks do not exhibit discernible splitting, indicating that the trigonal distortion of the RuX_6 octahedra is much smaller than the energy resolution of 80 meV . The result for RuBr_3 agrees with Raman scattering data [39]. The small trigonal distortion in the RuX_3 family contrasts with appreciable trigonal distortion in the Ir-based Kitaev candidates [40]. These observations establish $J = 1/2$ pseudospin physics in the RuX_3 family. Moreover, for insulating RuCl_3 and RuBr_3 whose pseudospin interactions are given in Eq. (1), the small trigonal distortion suggests small Γ' terms. Momentum dependence of the $J = 1/2$ intensity has yielded $\Gamma' = 0.1 \text{ meV}$ for RuCl_3 [24]. Future investigation of single crystals will allow the determination of Γ' term for RuBr_3 .

The intermediate energy range includes broad continua originating from intersite electron-hole excitations. The onset of the continuum is located at $\sim 1 \text{ eV}$ for RuCl_3 and 0.7 eV for RuBr_3 (vertical dashed lines), reaffirming their Mott-insulating nature [27]. In contrast, the continuum extends to zero energy in the metallic RuI_3 . As RIXS is a bulk-sensitive probe, our RIXS data provide spectroscopic evidence that the metallic transport of RuI_3 [29, 30] is not caused by the grain boundary in the polycrystalline samples but reflects its intrinsic bulk metallicity. This result agrees with metallic band structures observed by angle-resolved photoemission measurements [41]. The charge continuum overlaps with the intra-ionic $J = 3/2$ transitions, causing substantial lineshape broadening. However, the quasi-elastic $J = 1/2$ excitations remain sharply peaked, indicating that the onset of the continuum is located close to zero energy.

On top of the continuum, one identifies intra-ionic crystal-field transitions from the t_{2g}^5 ground state to the Hund's multiplets with the $t_{2g}^4 e_g^1$ electron configurations

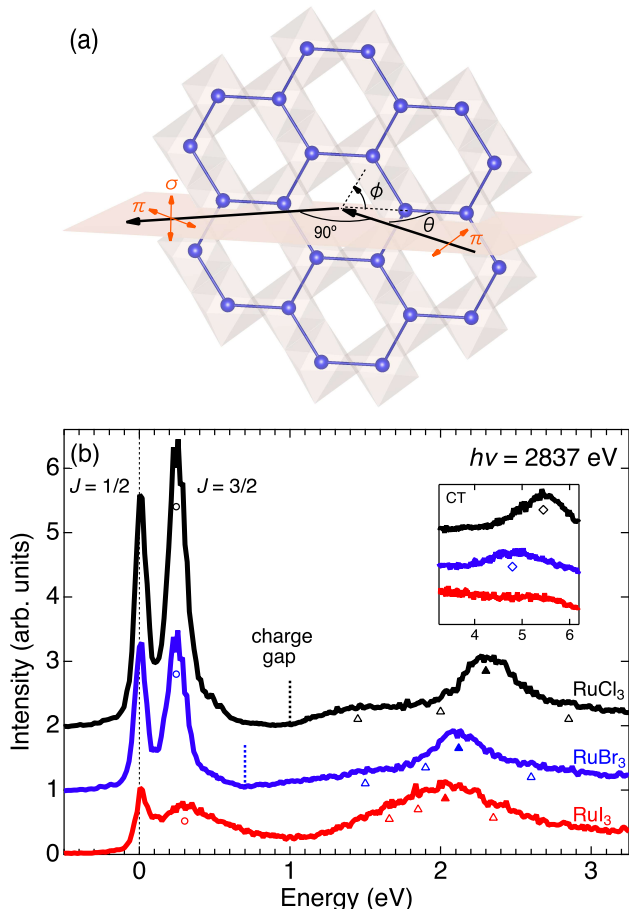


FIG. 2. (a) Scattering geometry for the resonant inelastic x-ray scattering (RIXS) experiment. The incident photons were π -polarized, and the σ - and π -polarized scattered photons were collected at the scattering angle of 90° . (b) Ru L_3 edge RIXS spectra of RuX_3 ($X = \text{Cl}, \text{Br}, \text{I}$) taken with the incident photons with $h\nu = 2837$ eV. The circles indicate $J = 3/2$ spin-orbit transitions. The vertical dashed lines indicate the onset energy of the intersite electron-hole continuum. Filled and open triangles indicate the main peak and shoulder structures from the crystal-field transitions to Hund's multiplets with $t_{2g}^4 e_g^1$ electron configurations. The inset shows the high-energy region containing charge-transfer (CT) excitations (squares).

(triangles). The energy of the main peaks (filled triangles) monotonically decreases as X changes from Cl to I. As this excitation energy is predominantly determined by the crystal field strength $10Dq$, the present data point to a systematic decrease of the $10Dq$ parameter. This appreciable change of the $10Dq$ parameter [$\Delta(10Dq) \geq 0.1$ eV, see Fig. 3(d)] is larger than that in the exfoliated nanosheets of RuCl_3 [$\Delta(10Dq) \lesssim 0.05$ eV] induced by surface strain [42], which has been proposed as another means to control the magnetism of the Kitaev magnets [43]. Furthermore, the energy separation of the shoulder structures (open triangles) decreases monotonically, indicating the monotonic reduction of the Hund's-rule

coupling constant J_H as discussed below.

The inset of Fig. 2(b) shows the high-energy region of the RIXS spectra including the charge transfer (CT) excitations (squares). The peak energy in RuBr_3 (~ 4.8 eV) is lower than that in RuCl_3 (~ 5.5 eV), reflecting the lower binding energy of the Br $4p$ orbitals in RuBr_3 than the Cl $3p$ orbitals in RuCl_3 . This leads to a stronger hybridization between the Ru $4d$ and Br $4p$ orbitals in RuBr_3 , as naturally expected from the increased spatial expansion of the Br $4p$ orbitals compared to the Cl $3p$ orbitals. The stronger hybridization results in the suppression of CT peak intensity and the reduction of the onset of the intersite charge continuum. This trend continues in RuI_3 . With the further enhancement of the hybridization between the Ru $4d$ and I $5p$ orbitals, RuI_3 no longer exhibits the CT peak. Instead, its high-energy spectral weight merges with the intersite charge continuum, which extends down to zero energy. The systematic enhancement of the d - p hybridization is well captured by electronic structure calculations [29, 44–47], which show the increase of the halogen p orbital contributions in the low-energy density of states as X goes from Cl to I.

To gain more insight into the evolution of d - p hybridization, Figs. 3(a)-(c) compare the RIXS intensity for RuX_3 taken with the t_{2g} resonance ($h\nu = 2837$ eV) and the e_g resonance ($h\nu = 2839$ eV). In all the RuX_3 systems, the latter condition diminishes the $J = 1/2$ and $J = 3/2$ transitions within the t_{2g}^5 sector. Concomitantly, it enhances the high-energy transitions involving the e_g orbitals in the Mott-insulating RuCl_3 and RuBr_3 . However, the resonance enhancement becomes less pronounced in RuBr_3 , and the metallic RuI_3 yields almost comparable RIXS intensity in the high-energy region (> 1 eV). We also observe the spectral weight shift in this region in RuI_3 , that is, the RIXS signal is more fluorescence-like due to the itinerancy of the final states. This indicates the e_g orbitals in RuI_3 show a large deviation from the Ru^{3+} ionic character due to the strong hybridization with the I $5p$ orbitals. Note that the ligand p orbitals more sensitively affect the Ru e_g orbitals than the t_{2g} orbitals, as the e_g orbitals point toward the halogen p orbitals.

We now quantify microscopic multiplet parameters in RuX_3 . For simplicity, we employ a d^5 ionic model Hamiltonian for the $4d$ electrons in a Ru^{3+} ion. It consists of the intra-atomic Coulomb interaction terms in the Kanamori form, H_C [48, 49], the intra-atomic spin-orbit coupling (SOC) H_{SOC} , and the cubic crystal field H_{cub} [50]. We employ spherical symmetry approximation of the interaction terms in H_C , which imposes the condition $U'_{mm'} = U - 2J_{H,mm'}$. This approximation makes the multiplet energies from the ground state independent of U in the ionic model with the fixed electron number $4d^5$. We do not include the trigonal crystal field given the absence of discernible splitting in the $J = 3/2$ transitions (Fig. 2). Free parameters are the crystal field strength

$10Dq$, the Hund's coupling between the t_{2g} orbitals J_H , and the SOC λ . The RIXS transition amplitude from the ground state was calculated within the dipole approximation and fast collision approximation [51, 52], which makes the transition amplitude independent of the incident x-ray energy. Powder averaging of the RIXS transition amplitudes was performed in the calculations for the polycrystalline RuBr_3 and RuI_3 [50].

The theoretical RIXS amplitudes for RuX_3 are shown in Figs. 3(a)-(c) as gray vertical bars. Each panel also includes the optimal parameters $10Dq$, J_H , and λ . Within the ionic model, the $J = 3/2$ transitions are located at the energy of $\sim 3\lambda/2$, which determines the λ parameter. For the Hund's multiplets involving the e_g orbitals, the energy of the main peak fixes the $10Dq$ parameter, and the energy separation of the shoulder structures determines J_H . It should be noted that the determined parameters represent "effective" values that incorporate the effect of the hybridization with the ligand p orbitals and the interaction with the charge continuum. The parameters for RuCl_3 agree with those estimated in the former study [24]. For the Mott-insulating RuCl_3 and RuBr_3 , the ionic model captures the multiplet structures of the RIXS data very well. On the other hand, the agreement remains qualitative in the metallic RuI_3 due to the strong mixing with the charge continuum. Yet, the overall phenomenology persists, allowing the estimation of the multiplet parameters.

The evolution of these multiplet parameters in RuX_3 is summarized in Fig. 3(d). First, we discuss the decreasing trend of $10Dq$ (top panel). The larger ionic radii of the heavier halogen elements lead to the expansion of the crystal lattice and the Ru-Ru distance d . At the same time, the outermost halogen p orbitals become more spatially extended. The decrease of the $10Dq$ parameter reveals that the crystal lattice expansion outweighs the expansion of the p orbitals, reducing the Coulomb repulsion between the Ru $4d$ and the halogen p electrons. The J_H parameter also shows a decreasing trend (middle panel). This indicates that the reduction of the charge gap enhances the screening of the Coulomb interactions. In the band picture, the enhanced d - p hybridization increases the overall bandwidth, which effectively reduces the electron correlations and induces the phase transition into the metallic state.

The well-defined $J = 1/2$ magnetic correlations in the metallic RuI_3 point to its proximity to the metal-insulator transition. In the archetypal $J = 1/2$ Mott insulator Sr_2IrO_4 [53], electron doping through La substitution at the Sr site induces a metallic state with backfolded Fermi surfaces [54, 55]. While the antiferromagnetic correlations become short-ranged with doping, the dispersion and intensity of the damped magnetic excitations remain analogous to the parent antiferromagnetic magnons [55, 56], allowing a "paramagnon" description of the magnetic dynamics akin to those in the hole-doped

cuprates [57–59]. On the other hand, the O K -edge RIXS spectra of the $4d^5$ paramagnetic metal Sr_2RhO_4 lack paramagnons at low energy, although the energy scale of the $J = 3/2$ excitons remains relevant [60]. The $J = 1/2$ magnetic correlations in RuI_3 thus provide spectroscopic evidence for its proximity to a magnetically ordered phase. This is in line with the metal-insulator transition at the doping level of $x \sim 0.85$ in $\text{Ru}(\text{Br}_{1-x}\text{I}_x)_3$ [31, 32]. The persisting magnetic fluctuations are likely responsible for the quasiparticle mass enhancement in the metallic region ($x > 0.85$), which is identified from the increase in the Sommerfeld coefficient upon approaching the phase boundary [31].

The bottom panel of Fig. 3(d) shows the evolution of the λ parameter. The insulating RuCl_3 and RuBr_3 have an identical $\lambda = 0.15$ eV. On the other hand, the hardening of $J = 3/2$ peak in RuI_3 leads to a larger $\lambda = 0.18$ eV. Note here that the increased d - p covalency reduces the orbital angular momentum of the t_{2g} electrons [48], which would yield the reduction of the λ parameter. Hence, additional effects need to be considered to describe the increasing trend. For this purpose, we consider the interaction with the charge continuum and the SOC of the I $5p$ orbitals. To clarify the former effect, we refer to the RIXS spectra of electron-doped $\text{Sr}_{2-x}\text{La}_x\text{IrO}_4$ [55]. While the lineshape broadening occurs with increasing doping, the energy of the $J = 3/2$ transitions remains almost identical across the insulator-metal transition. This suggests that interaction with a charge continuum alone does not induce appreciable hardening of the $J = 3/2$ transitions. The increase of the λ parameter in RuI_3 is thus primarily attributed to the SOC of the I $5p$ orbitals, which is activated via the strong mixing between the Ru t_{2g} and the I $5p$ orbitals. In general, honeycomb-lattice transition metal iodides have the potential to host higher-spin Kitaev magnetism utilizing the SOC splitting of the I $5p$ orbitals [61, 62]. Our results, therefore, suggest the important role of the I $5p$ orbitals in the low-energy magnetism of transition metal iodides.

In conclusion, we have presented Ru L_3 RIXS measurements of the multiplet structures of the Kitaev spin liquid candidates RuX_3 ($X = \text{Cl}, \text{Br}, \text{I}$). The RIXS spectra exhibit quasi-elastic magnetic correlations and spin-orbit transitions to the $J = 3/2$ states, establishing the $J = 1/2$ description of magnetism in the RuX_3 series. We also identified the gradual reduction of the intersite charge excitation gap, evidencing the bulk metallicity of RuI_3 . The multiplet analysis of the RIXS spectra reveals gradual suppression of electronic correlation as X goes from Cl to I, which is attributed to the increased bandwidth due to the enhanced d - p hybridization. Our results demonstrate the crucial role of halogen p orbitals in controlling the electronic properties of RuX_3 .

We thank R. Valentí and J. Nasu for enlightening discussions. This work was supported by Grants-in-Aid for Scientific Research from JSPS (KAKENHI) (numbers

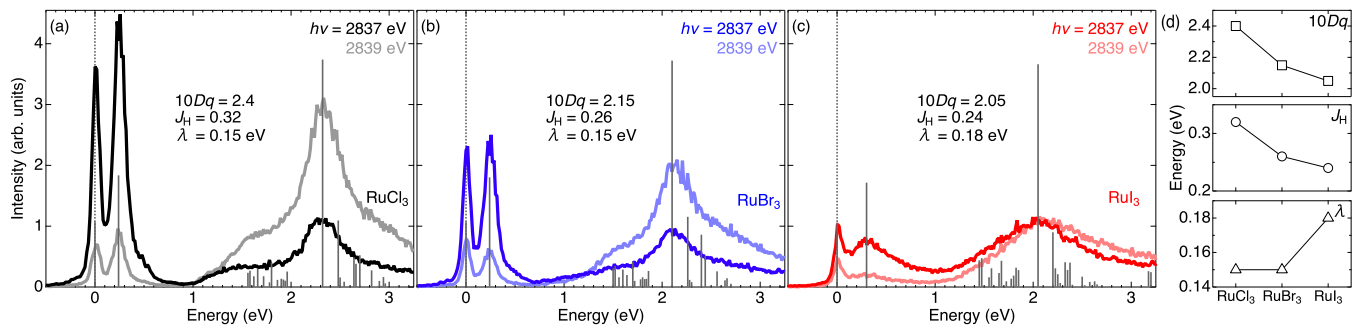


FIG. 3. (a)-(c) Comparison of RIXS intensity for RuX₃ taken with the t_{2g} resonance ($h\nu = 2837$ eV) and with the e_g resonance ($h\nu = 2839$ eV). The gray vertical bars indicate the theoretical RIXS intensity for the d^5 ionic model Hamiltonian [50]. (d) Evolution of the determined multiplet parameters $10Dq$, J_H , and λ for the RuX₃ series.

JP22K13994, JP22H00102, JP19H05823, JP19H05822, JP22H01175, JP22K18680), JST CREST (Grant No. JP19198318), and the European Research Council under Advanced Grant No. 669550 (Com4Com). We acknowledge DESY, a member of the Helmholtz Association HGF, for the provision of experimental facilities. The RIXS experiments were carried out at the beamline P01 of PETRA III at DESY. Sample growth at ISSP was carried out under the Visiting Researcher's Program (No. 202011-MCBXG-0006 and No. 202106-MCBXG-0073).

* hakuto.suzuki@tohoku.ac.jp

- [1] A. Kitaev, Anyons in an exactly solved model and beyond, *Ann. Phys.* **321**, 2 (2006).
- [2] G. Jackeli and G. Khaliullin, Mott Insulators in the Strong Spin-Orbit Coupling Limit: From Heisenberg to a Quantum Compass and Kitaev Models, *Phys. Rev. Lett.* **102**, 017205 (2009).
- [3] J. G. Rau, E. K.-H. Lee, and H.-Y. Kee, Spin-Orbit Physics Giving Rise to Novel Phases in Correlated Systems: Iridates and Related Materials, *Annu. Rev. Condens. Matter Phys.* **7**, 195 (2016).
- [4] M. Hermanns, I. Kimchi, and J. Knolle, Physics of the Kitaev Model: Fractionalization, Dynamic Correlations, and Material Connections, *Annu. Rev. Condens. Matter Phys.* **9**, 17 (2018).
- [5] H. Takagi, T. Takayama, G. Jackeli, G. Khaliullin, and S. E. Nagler, Concept and Realization of Kitaev Quantum Spin Liquids, *Nat. Rev. Phys.* **1**, 264 (2019).
- [6] H. Liu and G. Khaliullin, Pseudospin exchange interactions in d^7 cobalt compounds: Possible realization of the Kitaev model, *Phys. Rev. B* **97**, 014407 (2018).
- [7] R. Sano, Y. Kato, and Y. Motome, Kitaev-Heisenberg Hamiltonian for High-spin d^7 Mott Insulators, *Phys. Rev. B* **97**, 014408 (2018).
- [8] H. Liu, J. Chaloupka, and G. Khaliullin, Kitaev Spin Liquid in 3d Transition Metal Compounds, *Phys. Rev. Lett.* **125**, 047201 (2020).
- [9] F.-Y. Li, Y.-D. Li, Y. Yu, A. Paramakanti, and G. Chen, Kitaev materials beyond iridates: Order by quantum disorder and Weyl magnons in rare-earth double perovskites, *Phys. Rev. B* **95**, 085132 (2017).
- [10] J. G. Rau and M. J. P. Gingras, Frustration and anisotropic exchange in ytterbium magnets with edge-shared octahedra, *Phys. Rev. B* **98**, 054408 (2018).
- [11] S.-H. Jang, R. Sano, Y. Kato, and Y. Motome, Antiferromagnetic Kitaev interaction in f -electron based honeycomb magnets, *Phys. Rev. B* **99**, 241106(R) (2019).
- [12] Y. Motome, R. Sano, S. Jang, Y. Sugita, and Y. Kato, Materials design of Kitaev spin liquids beyond the Jackeli-Khaliullin mechanism, *J. Phys. Condens. Matter* **32**, 404001 (2020).
- [13] L. J. Sandilands, Y. Tian, K. W. Plumb, Y.-J. Kim, and K. S. Burch, Scattering Continuum and Possible Fractionalized Excitations in α -RuCl₃, *Phys. Rev. Lett.* **114**, 147201 (2015).
- [14] A. Banerjee, C. A. Bridges, J. Q. Yan, A. A. Aczel, L. Li, M. B. Stone, G. E. Granroth, M. D. Lumsden, Y. Yiu, J. Knolle, S. Bhattacharjee, D. L. Kovrizhin, R. Moessner, D. A. Tennant, D. G. Mandrus, and S. E. Nagler, Proximate Kitaev quantum spin liquid behaviour in a honeycomb magnet, *Nat. Mater.* **15**, 733 EP (2016).
- [15] A. Banerjee, J. Yan, J. Knolle, C. A. Bridges, M. B. Stone, M. D. Lumsden, D. G. Mandrus, D. A. Tennant, R. Moessner, and S. E. Nagler, Neutron scattering in the proximate quantum spin liquid α -RuCl₃, *Science* **356**, 1055 (2017).
- [16] S.-H. Do, S.-Y. Park, J. Yoshitake, J. Nasu, Y. Motome, Y. S. Kwon, D. T. Adroja, D. J. Voneshen, K. Kim, T. H. Jang, J. H. Park, K.-Y. Choi, and S. Ji, Majorana fermions in the Kitaev quantum spin system α -RuCl₃, *Nat. Phys.* **13**, 1079 EP (2017).
- [17] A. Banerjee, P. Lampen-Kelley, J. Knolle, C. Balz, A. A. Aczel, B. Winn, Y. Liu, D. Pajerowski, J. Yan, C. A. Bridges, A. T. Savici, B. C. Chakoumakos, M. D. Lumsden, D. A. Tennant, R. Moessner, D. G. Mandrus, and S. E. Nagler, Excitations in the field-induced quantum spin liquid state of α -RuCl₃, *npj Quantum Materials* **3**, 8 (2018).
- [18] Y. Kasahara, T. Ohnishi, Y. Mizukami, O. Tanaka, S. Ma, K. Sugii, N. Kurita, H. Tanaka, J. Nasu, Y. Motome, T. Shibauchi, and Y. Matsuda, Majorana quantization and half-integer thermal quantum Hall effect in a Kitaev spin liquid, *Nature* **559**, 227 (2018).
- [19] T. Yokoi, S. Ma, Y. Kasahara, S. Kasahara, T. Shibauchi, N. Kurita, H. Tanaka, J. Nasu, Y. Motome, C. Hickey, S.

- Trebst, and Y. Matsuda, Half-integer quantized anomalous thermal Hall effect in the Kitaev material candidate α -RuCl₃, *Science* **373**, 568 (2021).
- [20] J. A. Sears, M. Songvilay, K. W. Plumb, J. P. Clancy, Y. Qiu, Y. Zhao, D. Parshall, and Y.-J. Kim, Magnetic order in α -RuCl₃: A honeycomb-lattice quantum magnet with strong spin-orbit coupling, *Phys. Rev. B* **91**, 144420 (2015).
- [21] J. G. Rau, E. K.-H. Lee, and H.-Y. Kee, Generic Spin Model for the Honeycomb Iridates beyond the Kitaev Limit, *Phys. Rev. Lett.* **112**, 077204 (2014).
- [22] V. M. Katukuri, S. Nishimoto, V. Yushankhai, A. Stoyanova, H. Kandpal, S. Choi, R. Coldea, I. Rousochatzakis, L. Hozoi, and J. van den Brink, Kitaev interactions between $j = 1/2$ moments in honeycomb Na₂IrO₃ are large and ferromagnetic: insights from *ab initio* quantum chemistry calculations, *New J. Phys.* **16**, 013056 (2014).
- [23] J. A. Sears, L. E. Chern, S. Kim, P. J. Bereciartua, S. Francoual, Y. B. Kim, and Y.-J. Kim, Ferromagnetic Kitaev interaction and the origin of large magnetic anisotropy in α -RuCl₃, *Nat. Phys.* **16**, 837 (2020).
- [24] H. Suzuki, H. Liu, J. Bertinshaw, K. Ueda, H. Kim, S. Laha, D. Weber, Z. Yang, L. Wang, H. Takahashi, K. Fürsich, M. Minola, B. V. Lotsch, B. J. Kim, H. Yavaş, M. Daghofer, J. Chaloupka, G. Khaliullin, H. Gretarsson, and B. Keimer, Proximate ferromagnetic state in the Kitaev model material α -RuCl₃, *Nat. Commun.* **12**, 4512 (2021).
- [25] H. B. Cao, A. Banerjee, J.-Q. Yan, C. A. Bridges, M. D. Lumsden, D. G. Mandrus, D. A. Tennant, B. C. Chakoumakos, and S. E. Nagler, Low-temperature crystal and magnetic structure of α -RuCl₃, *Phys. Rev. B* **93**, 134423 (2016).
- [26] F. Ersan, E. Vatansever, S. Sarikurt, Y. Yüksel, Y. Kadioglu, H. D. Ozaydin, O. Üzengi Aktürk, Ümit Akıncı, and E. Aktürk, Exploring the electronic and magnetic properties of new metal halides from bulk to two-dimensional monolayer: RuX₃ (X = Br, I), *J. Magn. Magn. Mater.* **476**, 111 (2019).
- [27] Y. Imai, K. Nawa, Y. Shimizu, W. Yamada, H. Fujihara, T. Aoyama, R. Takahashi, D. Okuyama, T. Ohashi, M. Hagihala, S. Torii, D. Morikawa, M. Terauchi, T. Kawamata, M. Kato, H. Gotou, M. Itoh, T. J. Sato, and K. Ohgushi, Zigzag magnetic order in the Kitaev spin-liquid candidate material RuBr₃ with a honeycomb lattice, *Phys. Rev. B* **105**, L041112 (2022).
- [28] Y. Prots, S. Rößler, U. K. Rößler, H. Rosner, L. Akselrud, M. Schmidt, A. Fitch, and U. Schwarz, Crystal Structures and Twinning of RuBr₃, *Anorg. Allg. Chem.* **649**, e202300140 (2023).
- [29] K. Nawa, Y. Imai, Y. Yamaji, H. Fujihara, W. Yamada, R. Takahashi, T. Hiraoka, M. Hagihala, S. Torii, T. Aoyama, T. Ohashi, Y. Shimizu, H. Gotou, M. Itoh, K. Ohgushi, and T. J. Sato, Strongly Electron-Correlated Semimetal RuI₃ with a Layered Honeycomb Structure, *J. Phys. Soc. Jpn.* **90**, 123703 (2021).
- [30] D. Ni, X. Gui, K. M. Powderly, and R. J. Cava, Honeycomb-Structure RuI₃, A New Quantum Material Related to α -RuCl₃, *Adv. Mater.* **34**, 2106831 (2022).
- [31] F. Sato, H. Fujihara, H. Gotou, T. Aoyama, Y. Imai, and K. Ohgushi, Insulator-metal transition in Ru(Br_{1-x}I_x)₃ with honeycomb structure, *Phys. Rev. B* **109**, 035154 (2024).
- [32] D. Ni, X. Xu, and R. J. Cava, The layered RuBr₃-RuI₃ honeycomb system, arXiv:2311.13645 (2023).
- [33] Y. Sugita, Y. Kato, and Y. Motome, Antiferromagnetic Kitaev interactions in polar spin-orbit Mott insulators, *Phys. Rev. B* **101**, 100410(R) (2020).
- [34] K. Momma and F. Izumi, *VESTA3* for three-dimensional visualization of crystal, volumetric and morphology data, *J. Appl. Cryst.* **44**, 1272 (2011).
- [35] R. D. Johnson, S. C. Williams, A. A. Haghighirad, J. Singleton, V. Zapf, P. Manuel, I. I. Mazin, Y. Li, H. O. Jeschke, R. Valentí, and R. Coldea, Monoclinic crystal structure of α -RuCl₃ and the zigzag antiferromagnetic ground state, *Phys. Rev. B* **92**, 235119 (2015).
- [36] Y. Kubota, H. Tanaka, T. Ono, Y. Narumi, and K. Kindo, Successive magnetic phase transitions in α -RuCl₃: XY-like frustrated magnet on the honeycomb lattice, *Phys. Rev. B* **91**, 094422 (2015).
- [37] Y. Nagai, T. Jinno, J. Yoshitake, J. Nasu, Y. Motome, M. Itoh, and Y. Shimizu, Two-step gap opening across the quantum critical point in the Kitaev honeycomb magnet α -RuCl₃, *Phys. Rev. B* **101**, 020414(R) (2020).
- [38] H. Gretarsson, D. Ketenoglu, M. Harder, S. Mayer, F.-U. Dill, M. Spiwek, H. Schulte-Schrepping, M. Tischer, H.-C. Wille, B. Keimer, and H. Yavaş, IRIXS: a resonant inelastic X-ray scattering instrument dedicated to X-rays in the intermediate energy range, *J. Synchrotron Rad.* **27**, 538 (2020).
- [39] Y. Choi, J.-H. Lee, S. Lee, D. Wulferding, H. Fujihara, F. Sato, Y. Imai, K. Ohgushi, M.-J. Seong, and K.-Y. Choi, Magnetic and spin-orbit exciton excitations in the honeycomb lattice compound RuBr₃, *Phys. Rev. B* **106**, 174430 (2022).
- [40] H. Gretarsson, J. P. Clancy, X. Liu, J. P. Hill, E. Bozin, Y. Singh, S. Manni, P. Gegenwart, J. Kim, A. H. Said, D. Casa, T. Gog, M. H. Upton, H.-S. Kim, J. Yu, V. M. Katukuri, L. Hozoi, J. van den Brink, and Y.-J. Kim, Crystal-Field Splitting and Correlation Effect on the Electronic Structure of A₂IrO₃, *Phys. Rev. Lett.* **110**, 076402 (2013).
- [41] A. Louat, M. D. Watson, T. K. Kim, D. Ni, R. J. Cava, and C. Cacho, The pseudochiral Fermi surface of α -RuI₃, *Commun. Phys.* **7**, 43 (2024).
- [42] Z. Yang, L. Wang, D. Zhao, M. Luo, S. Laha, A. Güth, T. Taniguchi, K. Watanabe, B. V. Lotsch, J. H. Smet, M. Minola, H. Gretarsson, and B. Keimer, Resonant inelastic x-ray scattering from electronic excitations in α -RuCl₃ nanolayers, *Phys. Rev. B* **108**, L041406 (2023).
- [43] D. A. S. Kaib, S. Biswas, K. Riedl, S. M. Winter, and R. Valentí, Magnetoelastic coupling and effects of uniaxial strain in α -RuCl₃ from first principles, *Phys. Rev. B* **103**, L140402 (2021).
- [44] Y. Zhang, L.-F. Lin, A. Moreo, and E. Dagotto, Theoretical study of the crystal and electronic properties of α -RuI₃, *Phys. Rev. B* **105**, 085107 (2022).
- [45] D. A. S. Kaib, K. Riedl, A. Razpopov, Y. Li, S. Backes, I. I. Mazin, and R. Valentí, Electronic and magnetic properties of the RuX₃ (X = Cl, Br, I) family: two siblings—and a cousin?, *npj Quantum Mater.* **7**, 75 (2022).
- [46] L. Liu, K. Yang, G. Wang, D. Lu, Y. Ma, and H. Wu, Contrasting electronic states of RuI₃ and RuCl₃, *Phys. Rev. B* **107**, 165134 (2023).
- [47] S. Samanta, D. Hong, and H.-S. Kim, Electronic Structures of Kitaev Magnet Candidates RuCl₃ and RuI₃, *Nanomaterials* **14**, 9 (2024).

- [48] S. Sugano, Y. Tanabe, and H. Kamimura, *Multiplets of transition-metal ions in crystals* (Academic Press, New York, 1970).
- [49] A. Georges, L. d. Medici, and J. Mravlje, Strong Correlations from Hund's Coupling, *Annu. Rev. Condens. Matter Phys.* **4**, 137 (2013).
- [50] See Supplemental Material at @@link@@ for the details of the ionic model Hamiltonian and the powder averaging in the RIXS calculations.
- [51] L. J. P. Ament, M. van Veenendaal, T. P. Devereaux, J. P. Hill, and J. van den Brink, Resonant inelastic x-ray scattering studies of elementary excitations, *Rev. Mod. Phys.* **83**, 705 (2011).
- [52] B. J. Kim and G. Khaliullin, Resonant inelastic x-ray scattering operators for t_{2g} orbital systems, *Phys. Rev. B* **96**, 085108 (2017).
- [53] J. Kim, D. Casa, M. H. Upton, T. Gog, Y.-J. Kim, J. F. Mitchell, M. van Veenendaal, M. Daghofer, J. van den Brink, G. Khaliullin, and B. J. Kim, Magnetic Excitation Spectra of Sr_2IrO_4 Probed by Resonant Inelastic X-Ray Scattering: Establishing Links to Cuprate Superconductors, *Phys. Rev. Lett.* **108**, 177003 (2012).
- [54] A. de la Torre, S. McKeown Walker, F. Y. Bruno, S. Riccò, Z. Wang, I. Gutierrez Lezama, G. Scheerer, G. Giriat, D. Jaccard, C. Berthod, T. K. Kim, M. Hoesch, E. C. Hunter, R. S. Perry, A. Tamai, and F. Baumberger, Collapse of the Mott Gap and Emergence of a Nodal Liquid in Lightly Doped Sr_2IrO_4 , *Phys. Rev. Lett.* **115**, 176402 (2015).
- [55] H. Gretarsson, N. H. Sung, J. Porras, J. Bertinshaw, C. Dietl, J. A. N. Bruin, A. F. Bangura, Y. K. Kim, R. Dinnebier, J. Kim, A. Al-Zein, M. Moretti Sala, M. Krisch, M. Le Tacon, B. Keimer, and B. J. Kim, Persistent Paramagnons Deep in the Metallic Phase of $\text{Sr}_{2-x}\text{La}_x\text{IrO}_4$, *Phys. Rev. Lett.* **117**, 107001 (2016).
- [56] X. Liu, M. P. M. Dean, Z. Y. Meng, M. H. Upton, T. Qi, T. Gog, Y. Cao, J. Q. Lin, D. Meyers, H. Ding, G. Cao, and J. P. Hill, Anisotropic softening of magnetic excitations in lightly electron-doped Sr_2IrO_4 , *Phys. Rev. B* **93**, 241102(R) (2016).
- [57] M. Le Tacon, G. Ghiringhelli, J. Chaloupka, M. M. Sala, V. Hinkov, M. W. Haverkort, M. Minola, M. Bakr, K. J. Zhou, S. Blanco-Canosa, C. Monney, Y. T. Song, G. L. Sun, C. T. Lin, G. M. De Luca, M. Salluzzo, G. Khaliullin, T. Schmitt, L. Braicovich, and B. Keimer, Intense paramagnon excitations in a large family of high-temperature superconductors, *Nat. Phys.* **7**, 725 (2011).
- [58] M. P. M. Dean, G. Dellea, R. S. Springell, F. Yakhov-Harris, K. Kummer, N. B. Brookes, X. Liu, Y.-J. Sun, J. Strle, T. Schmitt, L. Braicovich, G. Ghiringhelli, I. Božović, and J. P. Hill, Persistence of magnetic excitations in $\text{La}_{2-x}\text{Sr}_x\text{CuO}_4$ from the undoped insulator to the heavily overdoped non-superconducting metal, *Nat. Mater.* **12**, 1019 (2013).
- [59] Y. Y. Peng, E. W. Huang, R. Fumagalli, M. Minola, Y. Wang, X. Sun, Y. Ding, K. Kummer, X. J. Zhou, N. B. Brookes, B. Moritz, L. Braicovich, T. P. Devereaux, and G. Ghiringhelli, Dispersion, damping, and intensity of spin excitations in the monolayer $(\text{Bi,Pb})_2(\text{Sr,L a})_2\text{CuO}_{6+\delta}$ cuprate superconductor family, *Phys. Rev. B* **98**, 144507 (2018).
- [60] V. Zimmermann, A. K. Yogi, D. Wong, C. Schulz, M. Bartkowiak, K. Habicht, L. Wang, M. Isobe, M. Minola, G. Khaliullin, B. Keimer, and M. Hepting, Coherent propagation of spin-orbit excitons in a correlated metal, *npj Quantum Mater.* **8**, 53 (2023).
- [61] P. P. Stavropoulos, D. Pereira, and H.-Y. Kee, Microscopic Mechanism for a Higher-Spin Kitaev Model, *Phys. Rev. Lett.* **123**, 037203 (2019).
- [62] P. P. Stavropoulos, X. Liu, and H.-Y. Kee, Magnetic anisotropy in spin-3/2 with heavy ligand in honeycomb Mott insulators: Application to CrI_3 , *Phys. Rev. Res.* **3**, 013216 (2021).